nature electronics

Article

https://doi.org/10.1038/s41928-024-01121-3

Ready-to-transfer two-dimensional materials using tunable adhesive force tapes

Received: 5 April 2023

Accepted: 10 January 2024

Published online: 9 February 2024

Check for updates

Maki Nakatani[1], Satoru Fukamachi[1], Pablo Solís-Fernández[1], Satoshi Honda[2], Kenji Kawahara[1,3], Yuta Tsuji[4,5], Yosuke Sumiya[6], Mai Kuroki[4], Kou Li[7,8], Qiunan Liu[9], Yung-Chang Lin[10], Aika Uchida[1], Shun Oyama[4], Hyun Goo Ji[4,12], Kenichi Okada[2], Kazu Suenaga[9], Yukio Kawano[7,8,11], Kazunari Yoshizawa[6], Atsushi Yasui[2] & Hiroki Ago[1,4] ✉

Graphene and other two-dimensional (2D) materials can be used to create electronic and optoelectronic devices. However, their development has been limited by the lack of effective large-area transfer processes. Here we report a transfer method that uses functional tapes with adhesive forces controlled by ultraviolet light. The adhesion of the tape is optimized for the transfer of monolayer graphene, providing a yield of over 99%. Once detached from the growth substrate, the graphene/tape stack enables easy transfer of graphene to the desired target substrate. The method can be used to transfer other 2D materials, including bilayer graphene, transition metal dichalcogenides, hexagonal boron nitride and stacked heterostructures. The solvent-free nature of the final release step facilitates transfer to various target substrates including flexible polymers, paper and three-dimensional surfaces. The tape/2D material stacks can also be cut into desired sizes and shapes, allowing site-selective device fabrication with reduced loss of 2D materials.

Two-dimensional (2D) materials have unique properties that can be used to create a range of novel devices[1]. Stacking 2D materials via artificial control of their van der Waals interaction allows new types of materials to be synthesized with a high degree of freedom in their compositions and twist angles[2]. Practical applications based on 2D materials and their heterostructures require transferring 2D materials at large scales and onto various target substrates, such as SiO_2/Si, patterned substrates and plastics[3–5]. Transfer is widely used for graphene[3,4] and hexagonal boron nitride (hBN)[6], whether they have been synthesized via chemical vapour deposition (CVD) on transition metal catalysts or exfoliated from their bulk forms. Transfer is also important for semiconducting transition metal dichalcogenides (TMDs), usually obtained on *c*-plane sapphire[7], and for 2D materials in general. However, the transfer process can degrade the electronic properties and quality of 2D materials, which affects the final device performance and increases process time and production cost[3–5]. This is typically through the introduction of atomic defects, macroscopic breaks, surface contamination and unintentional doping.

Various transfer processes have been explored to avoid such problems. The most widely used method to transfer CVD-grown 2D materials is to utilize thin support layers, such as polymethyl methacrylate (PMMA)[8,9], polystyrene[10], paraffin[11], rosin[12,13] and volatile

[1]Global Innovation Center (GIC), Kyushu University, Fukuoka, Japan. [2]Nitto Denko Corporation, Ibaraki, Japan. [3]Institute for 2D Materials LLC., Fukuoka, Japan. [4]Interdisciplinary Graduate School of Engineering Sciences, Kyushu University, Fukuoka, Japan. [5]Faculty of Engineering Sciences, Kyushu University, Fukuoka, Japan. [6]Institute for Materials Chemistry and Engineering (IMCE), Kyushu University, Fukuoka, Japan. [7]Laboratory for Future Interdisciplinary Research of Science and Technology, Tokyo Institute of Technology, Tokyo, Japan. [8]Department of Electrical, Electronic, and Communication Engineering, Faculty of Science and Engineering, Chuo University, Tokyo, Japan. [9]The Institute of Scientific and Industrial Research (ISIR-SANKEN), Osaka University, Osaka, Japan. [10]Nanomaterials Research Institute, National Institute of Advanced Industrial Science and Technology (AIST), Tsukuba, Japan. [11]National Institute of Informatics, Tokyo, Japan. [12]Present address: Semiconductor R&D Center, Samsung Electronics, Seoul, Republic of Korea. ✉e-mail: ago.hiroki.974@m.kyushu-u.ac.jp

molecule-PMMA composite[14]. Once the 2D layers are transferred with a polymer support, the supporting layer must be removed, usually by dissolving it with organic solvents. However, the polymer-mediated transfer usually leaves organic residues on the surface of the 2D material and also limits the choice of a target substrate[3,4]. Furthermore, transfer processes based on thin support layers can form wrinkles and cracks and are difficult to scale to large areas required for industrial processing. Thermal release tape (TRT) has been used as an alternative to thin support films, particularly for large-scale transfer[15,16]. Thin amorphous carbon and boron nitride layers have also been used as a sacrificial layer for transfer of a remote epitaxy film[17].

Stacks of 2D materials can be produced using polymer stamps (for example, polydimethylsiloxane), which allow for the deterministic stacking of layers with controlled sequencing order of the material and twist angles[18–20]. However, they are mainly limited to the transfer of small 2D flakes prepared by mechanical exfoliation. It is important for 2D materials research and their electronic applications to develop a more versatile and large-area transfer technique. For end users working with the applications of 2D materials, such as electronics, the technique should also be user-friendly, with simple processes that minimize the need for specialized equipment and can scale up to meet industrial demands.

In this Article, we show that functional tapes with an adhesive force tunable by ultraviolet (UV) light illumination can be used to transfer graphene and other 2D materials. Our straightforward method can produce large areas of high-quality, transferred monolayer graphene films with >99% yield and a room temperature carrier mobility of over 5,000 $cm^2 V^{-1} s^{-1}$. The method is also applicable to other 2D materials, including bilayer graphene (BLG), TMDs such as molybdenum disulfide (MoS_2) and tungsten disulfide (WS_2), and hBN by tuning the compositions of the adhesive layers and transfer procedures. We create a library of 2D materials tapes that are transferrable to various target surfaces including ceramics, paper and plastics. The tapes are flexible and can conform to different geometries, allowing the transfer to target substrates with non-planar surfaces. They also enable control of the twist angle of stacked 2D materials, similar to the pick-up stamp-based techniques used for exfoliated 2D materials.

Tape transfer of monolayer graphene

Figure 1a illustrates the transfer process using our functional tape, whose adhesive force is controlled by UV light (see Methods for details). First, we studied the transfer of high-quality monolayer graphene grown on a Cu(111) thin film[21,22]. The tape is attached on as-grown graphene, followed by UV light illumination. The UV light hardens the adhesive layer and at the same time greatly weakens the graphene–adhesive interaction, allowing the release of the graphene afterwards. The tape/graphene stack is then detached from the Cu(111) surface by electrochemical delamination, followed by washing with deionized water. To proceed with the transfer, the stack was gently placed on a SiO_2/Si substrate and baked at 90 °C. Finally, the tape is slowly peeled off the SiO_2 surface at 80 °C while leaving monolayer graphene on the SiO_2/Si (Supplementary Video 1).

As can be seen in the upper half of the optical image shown in Fig. 1b, monolayer graphene was transferred onto a SiO_2 surface without damages and contamination when the tape is exposed to UV light. In contrast, many breaks were observed in the unilluminated area, demonstrating the efficient control of adhesive force by UV light. This is explained by the large reduction of the adhesive force of the UV tape; UV light illumination reduced the adhesive force against a Si wafer from 0.5 N to 0.05 N for the tape with 10 mm width. As displayed in Supplementary Fig. 1, even millimetre-sized areas of graphene are almost free from structural defects, indicating high reliability of the transfer method. The UV-tape-assisted transfer is not restricted to graphene grown on Cu(111) and can also be applied to the transfer of monolayer graphene grown on polycrystal Cu foil and BLG grown on a Cu-Ni(111) film (Supplementary Figs. 2 and 3).

Isolated grains of graphene can be used to follow the transfer procedure. Figure 1c,d show the Cu and SiO_2 surfaces imaged before and after the electrochemical transfer of the hexagonal grains, respectively. On the Cu surface, the original location of graphene grains can be recognized, because the graphene prevents the oxidation of the covered Cu areas (Fig. 1c). As the graphene grains are also visible on the UV tape after the electrochemical delamination (Supplementary Fig. 4), we can monitor the quality of graphene throughout the whole transfer process by optical microscopy. As shown in Fig. 1d and Supplementary Fig. 5, the graphene grains were successfully transferred onto a SiO_2 surface without breaks, pinholes or wrinkling of their edges. In addition, no adhesive residue or particles were observed on the graphene surface, indicating very clean transfer.

To demonstrate the high reliability of our method, we conducted ten repetitions of the graphene transfer process using 10 × 20 mm substrates. As shown in Fig. 1e, our analysis reveals that all the transfer batches give an average yield of 98.2 ± 1.09%, with the highest value recorded at 99.3% (see Supplementary Figs. 6 and 7 for the details). Raman spectra of the transferred graphene (Fig. 1f) showed clear G and 2D bands at ~1,588 and ~2,680 cm^{-1}, respectively, with the intensity ratio of the 2D band to the G band (I_{2D}/I_G) being ~2. As can be seen in Fig. 1f and Supplementary Fig. 8, the defect-related D band observed at ~1,350 cm^{-1} is negligibly small, with the intensity ratio of the D band to G band (I_D/I_G) being less than 0.05 for the mapped area (Fig. 1g). This proves that the UV tape-transfer procedure did not induce damage to the graphene, because the UV illumination power required for the adhesive layer is sufficiently low and about half of the UV light is absorbed by the tape before reaching the graphene (Supplementary Fig. 9).

The electrical characteristics of UV tape-transferred graphene were investigated by fabricating field-effect transistors (FETs). Supplementary Fig. 10 shows representative transfer curves of the FETs measured at room temperature. The symmetric transfer curves suggest the hole and electron mobilities are similar. The field-effect carrier mobility was calculated for 95 devices, as shown in the histogram of Fig. 1h (top). The maximum mobility reached 5,696 $cm^2 V^{-1} s^{-1}$ and 4,793 $cm^2 V^{-1} s^{-1}$ for electrons and holes, respectively, with average values of 4,043 $cm^2 V^{-1} s^{-1}$ and 3,359 $cm^2 V^{-1} s^{-1}$. These average values are substantially higher than those of PMMA-transferred graphene (Fig. 1h (bottom)), being 3,031 $cm^2 V^{-1} s^{-1}$ and 3,106 $cm^2 V^{-1} s^{-1}$ for electrons and holes, respectively[23]. Therefore, the electrical measurement confirmed the high quality of the graphene transferred by our UV tape. Recently, UV tape has been used for the transfer of graphene, but with rosin used as a protecting layer for the graphene, which needs to be removed afterwards[13]. Although the UV light facilitates the rosin removal, FETs fabricated with the transferred graphene showed high p doping, which suggests the presence of residues on the graphene surface[13].

The UV tape allows the fabrication of stacks of monolayer graphene, as displayed in Fig. 1i. Three large graphene sheets of up to 50 × 50 mm were sequentially transferred onto SiO_2 using three UV tapes (Supplementary Fig. 11), demonstrating the potential of our method to produce vertically stacked 2D structures at large scales. In addition, the mechanically robust UV tapes makes the large-area transfer easier and more reproducible. Supplementary Fig. 12 and Supplementary Video 2 show the successful transfer of 4 inch monolayer graphene.

Comparison with other transfer methods

In Fig. 2a–f and Supplementary Fig. 13, the monolayer graphene transferred with UV tape is compared with those transferred with PMMA, which is the most widely used protective layer[8,9,21–23], and with the TRT used to transfer large-area monolayer graphene sheets due to its convenience[15,16]. The graphene transferred with the UV tape (Fig. 2a) shows a much cleaner surface with lower density of breaks than that transferred

https://doi.org/10.1038/s41928-024-01121-3

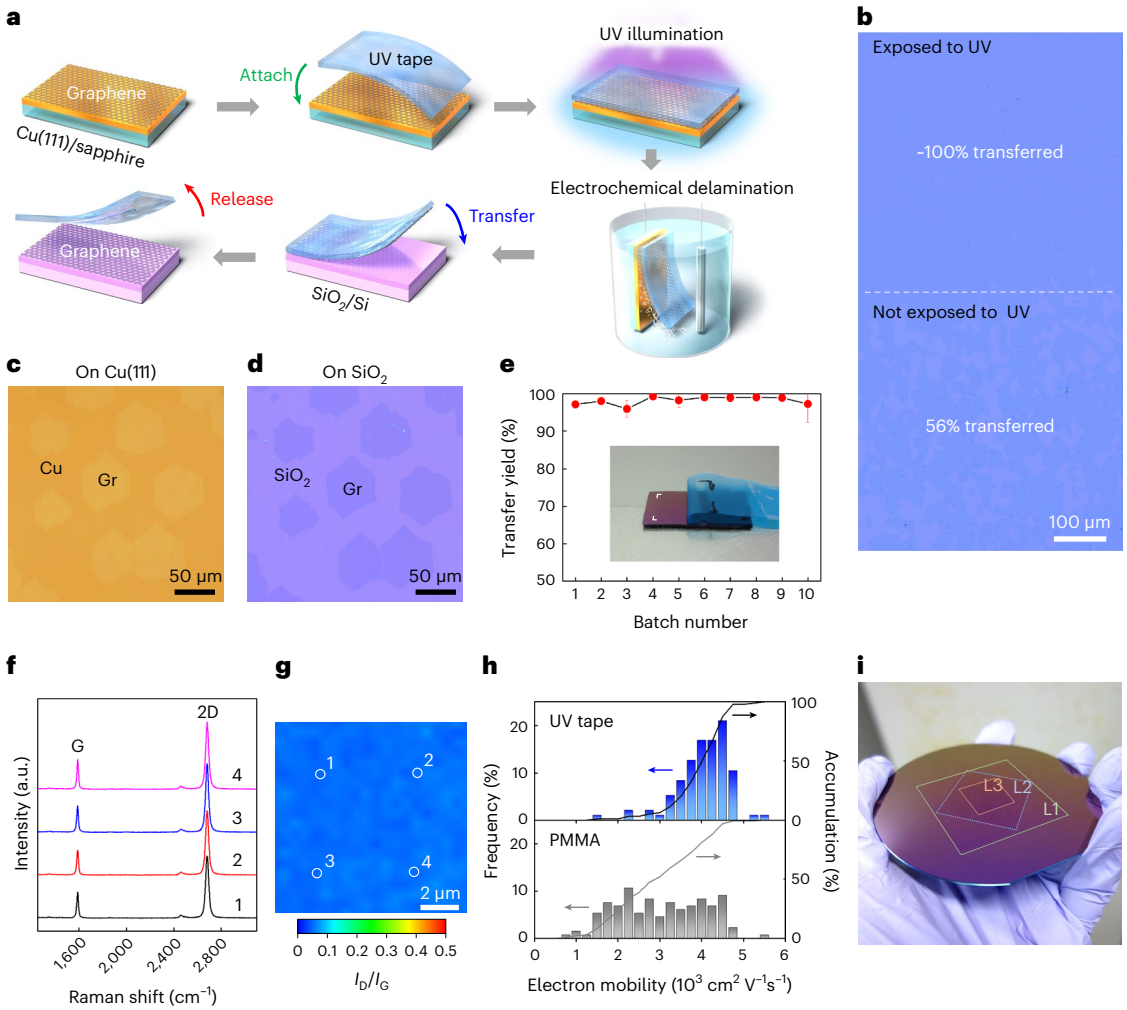

Fig. 1 | UV tape-assisted transfer of monolayer graphene and its characterizations. a, Transfer process of monolayer graphene from Cu(111)/sapphire to a SiO_2/Si substrate using the UV tape. **b**, Optical micrograph of a transferred graphene sheet. The upper half was exposed to the UV light, while the lower half was kept dark. These images indicate that the UV light is essential for the uniform transfer of graphene. **c**,**d**, Optical images of the as-grown Cu surface with aligned graphene grains (**c**) and the graphene grains after transfer onto SiO_2 (**d**). **e**, Transfer yield of a monolayer graphene sheet calculated for 10 transfer batches. Inset is a photograph showing the removal of the UV tape, leaving graphene on the surface of a SiO_2/Si substrate (10 × 20 mm^2). **f**,**g**, Raman spectra (**f**) and mapping of the I_D/I_G intensity ratio (**g**) of a transferred graphene sheet. The numbers in **f** indicate the measured positions in **g**. **h**, Histograms of the electron mobilities of the graphene FETs. The monolayer graphene was transferred with the UV tape (upper) and PMMA (lower). The measurement was conducted at room temperature. **i**, Photograph of graphene stack made by transferring three sheets of large monolayer graphene, where L1, L2 and L3 correspond to the first, second and third transferred graphene layers, respectively. a.u., arbitrary units.

with PMMA (Fig. 2b). The TRT transfer induced damage in the graphene and left many residues from the adhesive (Fig. 2c). The TRT contains a heat-sensitive foaming agent in the adhesive layer to release the graphene, and the resulting foam severely damaged the graphene (see Supplementary Fig. 14 for the optical image of the tape surface).

Atomic force microscopy (AFM) images of the UV-tape-transferred graphene (Fig. 2d and Supplementary Fig. 13a) also prove that the graphene surface is almost free from impurities, with a roughness average (R_a) of 0.24 nm, confirming the clean transfer of monolayer graphene. In contrast, the PMMA-transfer induced some breaks in the graphene (Fig. 2e and Supplementary Fig. 13b), while the TRT left a high density of adhesive residues on the graphene surface (Fig. 2f and Supplementary Fig. 13c). The UV tape also showed a much sharper height distribution of the AFM images (Fig. 2g) than those of PMMA and TRT. As seen in Supplementary Fig. 13d, the surface roughness (R_a) of the UV-tape-transferred graphene is much smaller than that of PMMA-transferred graphene. We therefore conclude that the UV tape transfer gives higher-quality graphene than that using PMMA and TRT.

The presence of contamination and residues due to the UV tape was studied by X-ray photoelectron spectroscopy (XPS) analysis of both the graphene and tape surfaces (Fig. 2h and Supplementary Table 1). While the adhesive layer of the UV tape contains N atoms, the N peak intensity was below the detection limit for the graphene after being transferred onto a SiO_2 surface (Fig. 2h). This result also reflects the clean transfer without tape residue on the graphene surface. From the Raman 2D–G plot shown in Extended Data Fig. 1, the p-type doping induced by the PMMA and TRT was found to be suppressed in the graphene transferred by the UV tape, while there was no notable change in the strain.

Mechanism of UV-assisted transfer

In this work, we used specifically designed UV-sensitive adhesives coated on polyolefin sheets. The adhesive is a random copolymer prepared by polymerization of three types of monomers, as shown in Supplementary Table 2. The composition and thickness were optimized with the aid of machine learning (least absolute shrinkage and selection

https://doi.org/10.1038/s41928-024-01121-3

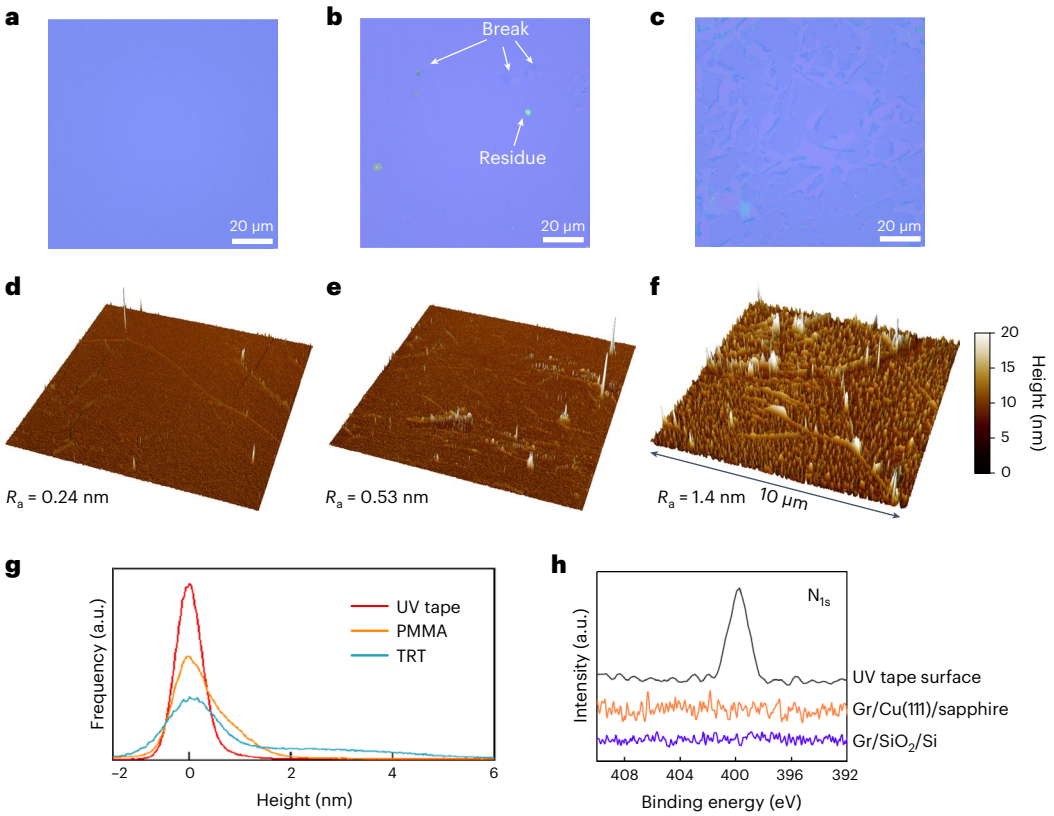

Fig. 2 | Comparison with other transfer methods. a–**g**, Optical (**a**–**c**) and AFM (**d**–**f**) images of graphene transferred with UV tape (**a**,**d**), PMMA film (**b**,**e**) and TRT (**c**,**f**). **g**, Height distributions calculated from the AFM images in **d**–**f**. **h**, XPS N_{1s} spectra measured for the tape surface, as-grown graphene on Cu(111)/sapphire and transferred graphene onto a SiO_2/Si substrate.

operator) to obtain suitable ratios of the monomers, concentrations of photopolymerization initiator and crosslinking agents for graphene transfer. Details of the machine learning-based optimization are presented in Supplementary Fig. 15.

Before the UV illumination, the adhesive of the UV tape is sufficiently soft to spread uniformly over the graphene surface. This promotes effective contact between the adhesive layer and the graphene, enabling full transfer of the graphene. The UV illumination in the presence of the initiator induces a crosslinking reaction of the methacrylic groups existing in one of the monomers, generating a network of the random copolymers, as illustrated in Fig. 3a. This hardens the adhesive layer, contributing to the detachment of graphene in the following releasing step. If the adhesive remains viscous or rubbery, mechanical deformations of the adhesive would induce unwanted breakages of graphene with residual adhesive.

In the case of conventional polymer support layers, such as PMMA, a thin film consisting of isolated polymer chains is used. This polymer layer is finally dissolved with organic solvent, but some polymer chains (either isolated chains or entangled multiple polymers) tend to remain on the graphene surface. However, in our UV tape, we used a cross-linked copolymer as the adhesive layer so that polymer chains are tightly bound with each other. Therefore, polymer residue can be strongly suppressed. In addition, the UV light illumination further promotes the crosslinking (Fig. 3a), thus facilitating residue-free transfer.

As a result, PMMA film needs to be very thin, because it needs to be removed in the final transfer step. Such thin PMMA film cannot completely prevent breakage and pinhole formation in the graphene during an electrochemical bubbling process. In contrast, in our UV tape, the adhesive layer is supported by ~100-μm-thick polyolefin substrate, so the formation of breakages and pinholes is strongly suppressed.

To gain insights into the change of the adhesion force induced by UV illumination, we performed density functional theory (DFT) calculations. We compared the physisorption of the monomer model consisting of two monomer structures with methacrylic groups (Fig. 3b and Supplementary Fig. 16a) and their dimer forms (Fig. 3c and Supplementary Fig. 16b) to study the change in van der Waals interaction caused by polymerization. First, the geometric configurations of these molecules as well as their distances to the basal graphene surface were optimized. The adhesion force can be estimated by fitting the change in energy (E) with respect to the adsorbate moving away from the surface with the Morse potential function[24,25]

$$E = E_{\mathrm{ad}}\left(1 - e^{-a\Delta r}\right)^2 \quad (1)$$

where E_{ad} is the depth of the potential well that corresponds to the adsorption energy, a is a constant that determines the width of the potential well and Δr is the vertical distance from the equilibrium position. The maximum adhesion force F_{max} can be expressed as follows:

$$F_{\mathrm{max}} = \frac{1}{2} a E_{\mathrm{ad}} \quad (2)$$

As shown in Fig. 3d, the F_{max} value for the dimer model is smaller than that of the monomer model. The adsorption energy of the dimer (0.688 eV) is also smaller than that of the two monomers (0.925 eV). A more detailed analysis of the DFT results is listed in Supplementary Table 3. We also performed the DFT calculation for the polymerization of ethylene molecules on the graphene surface (Supplementary Fig. 17) and obtained a tendency similar to the dimerization shown in Fig. 3b–d. The attractive π–π interaction between the monomer and graphene

https://doi.org/10.1038/s41928-024-01121-3

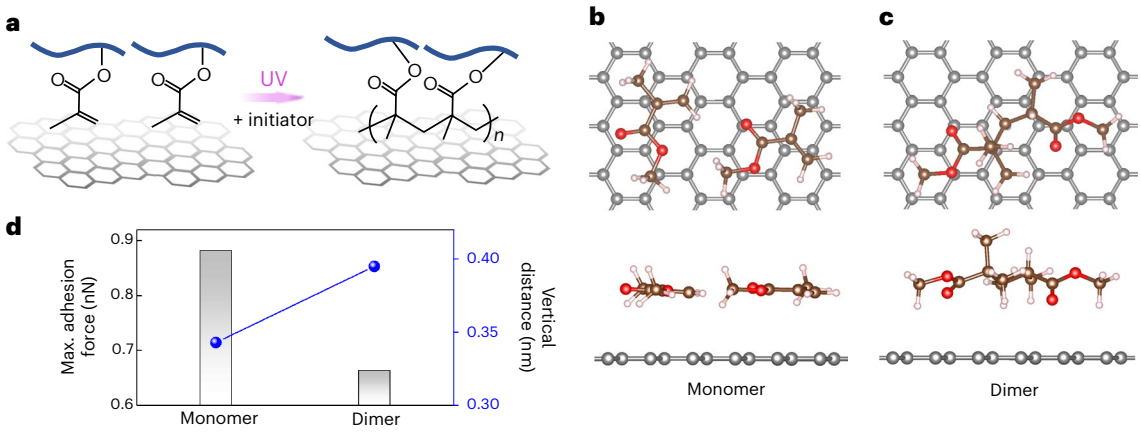

Fig. 3 | Mechanism of UV tape-assisted graphene transfer. a, Schematic of the polymerization reaction induced by UV light in the presence of a photopolymerization initiator. **b**,**c**, Models of molecules used to calculate the adhesion force of the UV tape to graphene. Monomer (**b**) and dimer (**c**) represent the chemical structures of the side chain of the adhesive copolymer before and after the photopolymerization, respectively. Upper and lower panels show the top and side views, respectively. Red, brown and pink are O, C and H atoms, respectively, and grey are C atoms of graphene. **d**, Comparison of maximum adhesion force (grey) and vertical distance between graphene and the molecules (blue). The vertical distance was measured using the coordinates of the centre of gravity of the molecules. Max, maximum.

is lost upon the polymerization, increasing the equilibrium distance and weakening the adsorption. In addition, UV-induced polymerization occurs accompanied by the morphological change of the polymer network, which leads to hardening of the adhesive layer. Therefore, we think that mechanical hardening of the adhesive layer as well as reduction of graphene–adhesive interaction allows us to transfer the graphene sheet from the UV tape to SiO_2 without apparent damage to the graphene.

The adhesive force between the graphene and the substrate was experimentally studied by scratching the graphene with the tip of a cantilever of a friction force microscope (Supplementary Fig. 18). The measurements indicated that the adhesion of graphene to the UV tape after illumination is much weaker than that of graphene on Cu(111) and SiO_2 substrates. This explains why monolayer graphene can be released onto a SiO_2 substrate from the UV tape in the final step.

Transfer of TMDs and fabrication of 2D heterostructures

By optimizing the composition of the adhesive layer, CVD-grown TMDs were also successfully transferred from their growth substrates (sapphire) to SiO_2/Si substrates without contamination. Figure 4a shows optical images of triangular MoS_2 grains (left) and a continuous MoS_2 sheet (right) taken after the tape transfer (see Supplementary Fig. 19 for more optical images). The composition of the adhesive differs from that used for graphene, as it was specifically tuned to transfer TMDs (see Supplementary Table 2 for details). The adhesive force of this tape changes from 1.25 N per 10 mm to 0.1 N per 10 mm by the UV light. As-grown MoS_2 was mechanically peeled off the growth substrate (in our case, sapphire) with the aid of water[10], as electrochemical delamination is not possible on sapphire. Similar to the graphene transfer, the MoS_2 transferred with the UV tape possessed a clean surface, while the surface of the PMMA-transferred MoS_2 was covered with polymer residue (Supplementary Fig. 20). As shown in Fig. 4b, the tape-transferred MoS_2 exhibited n-type semiconducting behaviour, with a high electron mobility of 23 $cm^2 V^{-1} s^{-1}$ (average mobility is 8.5 $cm^2 V^{-1} s^{-1}$) and an on/off ratio of $>10^6$. The high carrier mobility indicates that the quality of the monolayer MoS_2 is maintained even after the transfer with UV tape. Data for other devices and comparison with previous literature of the CVD MoS_2 devices are presented in Supplementary Fig. 21 and Supplementary Table 4, respectively.

As mentioned later, unlike PMMA-mediated transfer, the final releasing step does not require solvent so that we can fabricate TMD devices on flexible plastic substrates. In addition, as the UV tape is more mechanically robust than PMMA, we can apply this tape transfer to large-area TMD wafers and cut it into small pieces from a large TMD wafer. In addition, the MoS_2 surface was found to be cleaner than that transferred by PMMA (Supplementary Fig. 20). More importantly, the releasing step is very simple: the UV tape/2D material stack is placed on a target substrate, and the tape is slowly removed. This simple releasing step greatly helps end users to develop their own electronic devices.

The UV tape method also allows us to fabricate heterostacks of TMDs. Figure 4c and Supplementary Fig. 22 show optical images of a heterostack of MoS_2 on WS_2, produced by the sequential transfer to a SiO_2 substrate. Figure 4d and Extended Data Fig. 2 display scanning transmission electron microscope (STEM) images of the cross-section of the MoS_2/WS_2 heterostack. Clear atomic structures of both MoS_2 and WS_2 are recognized in Fig. 4d, with a clean van der Waals interface that is free from contaminants. The corresponding electron energy loss spectroscopy (EELS) elemental mappings (lower panels of Fig. 4d) confirm the presence of both MoS_2 and WS_2.

Figure 4e shows the Raman spectra of MoS_2, WS_2 and their overlapped region. The photoluminescence (PL) spectra measured at the same regions (Fig. 4f) exhibit a strong quenching of the WS_2 PL in the overlapped area, indicating strong interlayer coupling between MoS_2 and WS_2[26], reflecting the clean interface of the 2D heterostack.

Transfer of multilayer hBN for graphene heterostacks

Our transfer method is also applicable to large-area multilayer hBN grown by CVD[23]. As shown in Fig. 4g,h, two sheets of multilayer hBN and one of monolayer graphene of different sizes were successively transferred onto a SiO_2 substrate using UV tapes. This allows us to study four different configurations by Raman spectroscopy on a single SiO_2 substrate: hBN/Gr/hBN, hBN/Gr, Gr/hBN and Gr (note that in the notation for the stacks, the material on the left is located on the top of the stacks). Typical Raman spectra of the graphene in each configuration are shown in Fig. 4i, in which graphene G and 2D bands as well as hBN E_{2g} band are observed. Figure 4j and Supplementary Fig. 23 display the Raman intensity mappings of the hBN E_{2g} band. The data from Raman measurements confirmed successful preparation of the graphene–hBN heterostacks. The graphene 2D band becomes stronger when graphene

https://doi.org/10.1038/s41928-024-01121-3

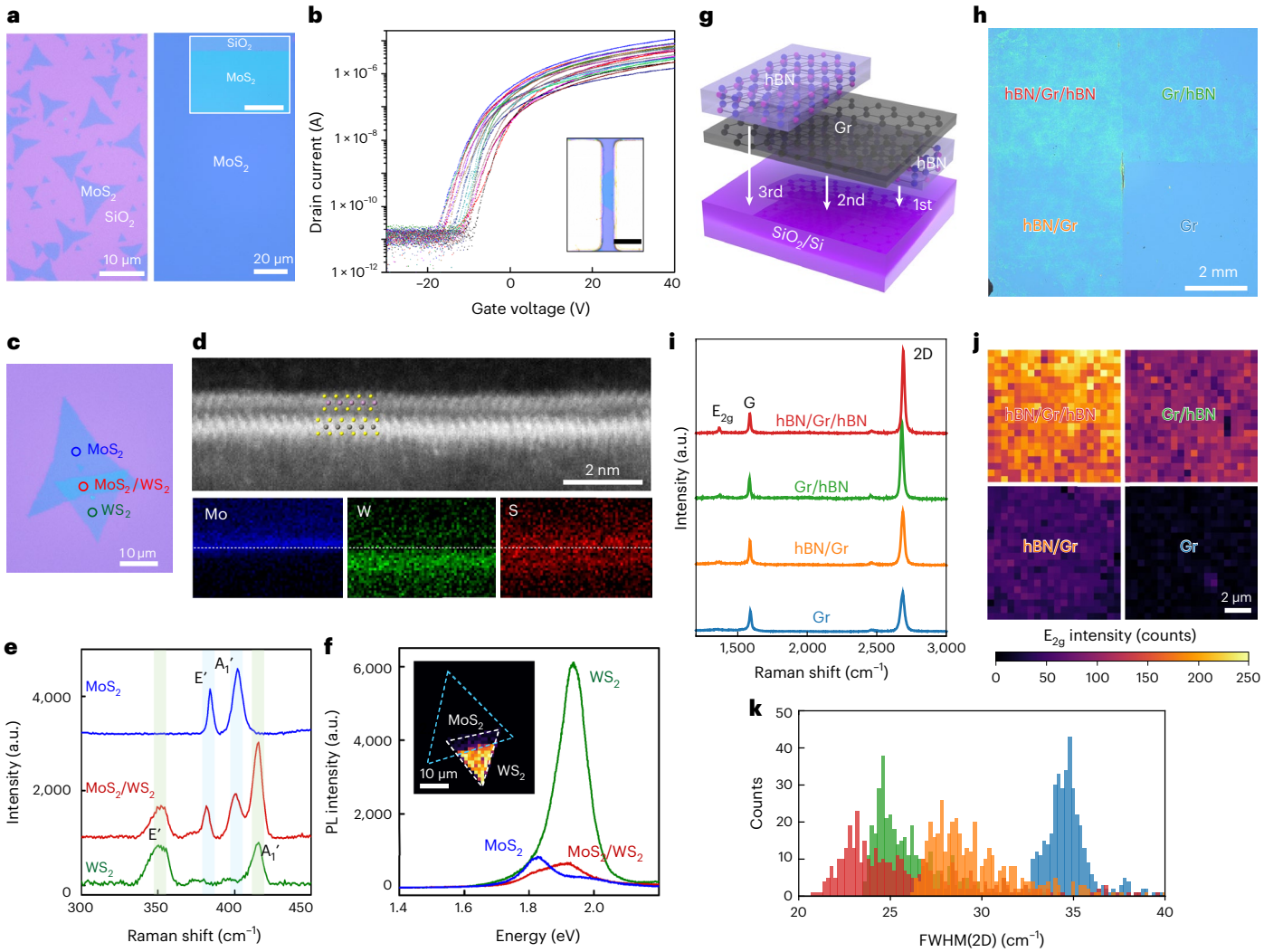

Fig. 4 | Transfer of other 2D materials and fabrication of stacked heterostructures. a, Optical image of monolayer MoS_2 transferred onto a SiO_2 substrate using UV tape (left, isolated MoS_2 grains; right, continuous MoS_2 film). Inset: low-magnification image of the continuous MoS_2 film (scale bar, 1 mm). **b**, Transfer curves of MoS_2 transistors. Inset: optical image of one of the device channels (scale bar, 10 μm). **c**, Optical image of a MoS_2/WS_2 heterostructure made by sequential transfer of MoS_2 and WS_2 onto SiO_2. **d**, STEM image of the cross-section of the MoS_2/WS_2 heterostack (top) and EELS elemental mapping images for Mo, W and S (bottom). **e**,**f**, Raman (**e**) and PL (**f**) spectra of MoS_2, WS_2 and their heterostructure collected from the areas indicated in **c**. Inset in **f** is the PL intensity map of WS_2, indicating strong PL quenching of the WS_2 at the overlapped area. **g**, Schematic of the successive transfer of multilayer hBN, graphene and hBN onto a SiO_2/Si substrate. **h**, Optical image of the graphene–hBN heterostacks fabricated on a single SiO_2/Si substrate. **i**, Representative Raman spectra measured at the four different regions of **h**. **j**, Raman mapping images of the intensity of the hBN E_{2g} band. **k**, Histogram of the FWHM(2D) distribution of graphene. The colours are the same as used for **i**.

is stacked with multilayer hBN, especially when the hBN is situated underneath the graphene (Fig. 4i). As the full-width at half-maximum of the 2D band (FWHM(2D)) is sensitive to strain and doping of the graphene[27,28], it can be used to monitor the screening effect by hBN multilayers. The FWHM(2D) of graphene is the narrowest in the hBN/Gr/hBN structure (red in Fig. 4k), indicating that the sandwich structure is the most effective to screen out the influences of both the SiO_2 substrate and gas adsorption. The graphene-on-hBN (Gr/hBN, green) has a narrower 2D band than that with hBN on top (hBN/Gr, orange). This indicates that the influence of the SiO_2 substrate is stronger than that of surface gas adsorption.

The transfer of 2D materials onto SiO_2 using various methods is a well-established practice. For example, the transfer process can be facilitated by modifying the hydrophilicity of the SiO_2 surface. However, there are surfaces onto which the transfer of 2D materials can be challenging, such as a Si substrate without a top SiO_2 layer. As shown in Supplementary Fig. 24, it is difficult to fully transfer multilayer hBN onto a Si substrate using a PMMA support layer, as the hBN is partly removed or broken when the PMMA is dissolved in acetone due to the weak adhesion between the hBN and the Si surface. However, as the tape method does not require any solvent, we could transfer hBN on such an inert Si surface (Supplementary Fig. 24).

Cut-and-transfer method for patterned transfer of 2D materials

In practical devices utilizing 2D materials, such as photosensors, the total active area of the 2D materials required in one wafer is usually very small. Hence, when transferring a large sheet of 2D material, most of the area needs to be removed by lithography and etching processes to leave small channels at predesigned positions. UV tape transfer allows for an easy way to economize 2D materials by cutting the tape with the 2D material already on it into small pieces with suitable sizes and shapes. These pieces can then be transferred at the desired positions.

https://doi.org/10.1038/s41928-024-01121-3

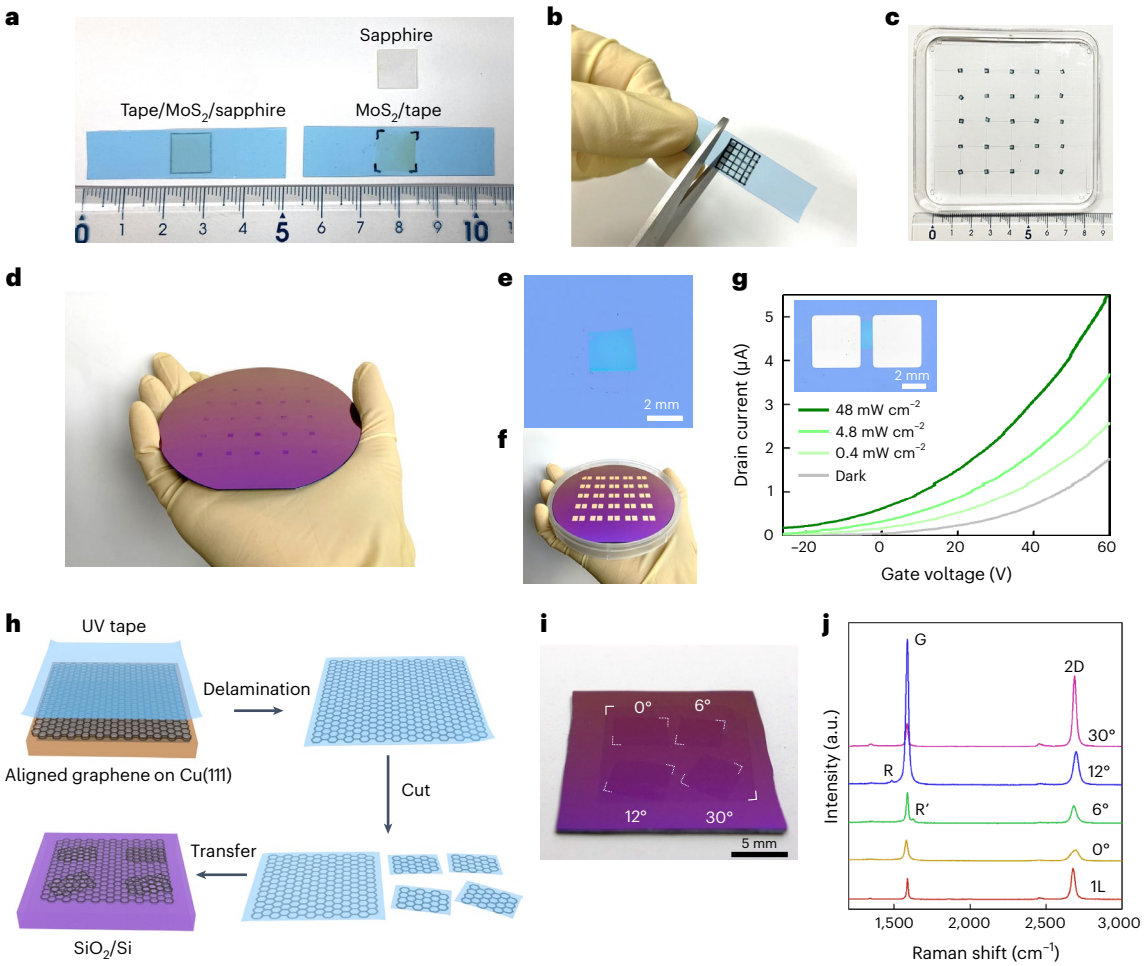

Fig. 5 | Cut-and-transfer process of MoS_2 and graphene. a, Photograph of the delaminated MoS_2/tape from a sapphire substrate with the UV tape. **b**, Cutting the MoS_2/tape with scissors. **c**, Resulting small pieces of the MoS_2/tape ready for transfer. **d**, Transferred MoS_2 pattern on a 4 inch SiO_2 substrate. **e**, Optical image of transferred 2.5 × 2.5 mm^2 MoS_2. **f**, Final device array. **g**, Photoresponse of the patterned MoS_2 FET under the specified illumination power densities. Inset: one of the MoS_2 FETs. **h**, Concept of artificially stacked BLG made by the cut-and-transfer method. Using large, oriented monolayer graphene grown on Cu(111)/sapphire, the BLG stack was made by transferring the cut tapes. **i**, Photograph of the artificially stacked BLG. **j**, Representative Raman spectra of monolayer graphene (1L) and bilayer graphene with the four stacking angles.

To prove this concept, a UV tape holding monolayer MoS_2 was cut into small pieces (2.5 × 2.5 mm^2) (Fig. 5a–c). After placing the tape/MoS_2 pieces on a SiO_2 substrate using a guide, each tape was removed while heating the SiO_2 substrate at 80 °C. Owing to their mechanical robustness, small-sized UV tape pieces are easier to handle than the PMMA used in a previous work[29]. This ease of processing of the UV tape-transfer process makes it a prime candidate for automated processing[20], enabling improved transfer precision, quality and yield. Figure 5d,e and Supplementary Fig. 25 show the pattern of monolayer MoS_2 fabricated on a 4 inch SiO_2 wafer. Metal electrodes were evaporated through a shadow mask for the fabrication of MoS_2 FETs (Fig. 5f). The patterned MoS_2 device showed n-type carrier transfer and clear photoresponse to visible light (532 nm wavelength), as shown in Fig. 5g. The cut-and-transfer process described here can greatly reduce the required area of 2D materials, thus decreasing production costs associated with synthesizing 2D materials at wafer scales.

The proposed cut-and-transfer method also allows precise control over the twist angle of stacked 2D layers, analogous to the polymer stamp methods currently used to produce stacks of exfoliated materials[30]. With this method, we fabricated large areas of twisted BLG with controlled twist angles. Employing a large sheet of oriented monolayer graphene grown on Cu(111)/sapphire allows us to cut and stack graphene sheets while controlling the twist angles, as illustrated in Fig. 5h. Figure 5i shows a photograph of the artificially stacked BLG made with the orientation-controlled monolayer graphene, in which four small pieces and one large sheet of monolayer graphene were stacked by using the UV tapes. The robustness of the tape allows us to cut and handle small pieces of graphene while preserving their initial angle, allowing the twist angle to be defined. The resulting Raman spectra taken at different stacks (Fig. 5j) evidence characteristic signatures of the given twist angles[31] supporting that the twist angle is well controlled by our method.

Tape transfer on various targets and application to infrared and THz sensors

Our findings are developed to make a library of 2D tapes, which can be available for end users, as displayed in Fig. 6a and Extended Data Fig. 3. To demonstrate the wide applicability and effectiveness of the UV tape-transfer method, we transferred graphene and TMDs on a variety of substrates. Monolayer graphene was transferred onto the surface of a ceramic mug (Fig. 6b and Supplementary Fig. 26), evidencing that the UV tape allows us to transfer onto curved surfaces of non-ideal materials. The UV tape transfer is also gentle enough to allow the transfer of 2D materials over free-standing areas. This is demonstrated by the transfer

https://doi.org/10.1038/s41928-024-01121-3

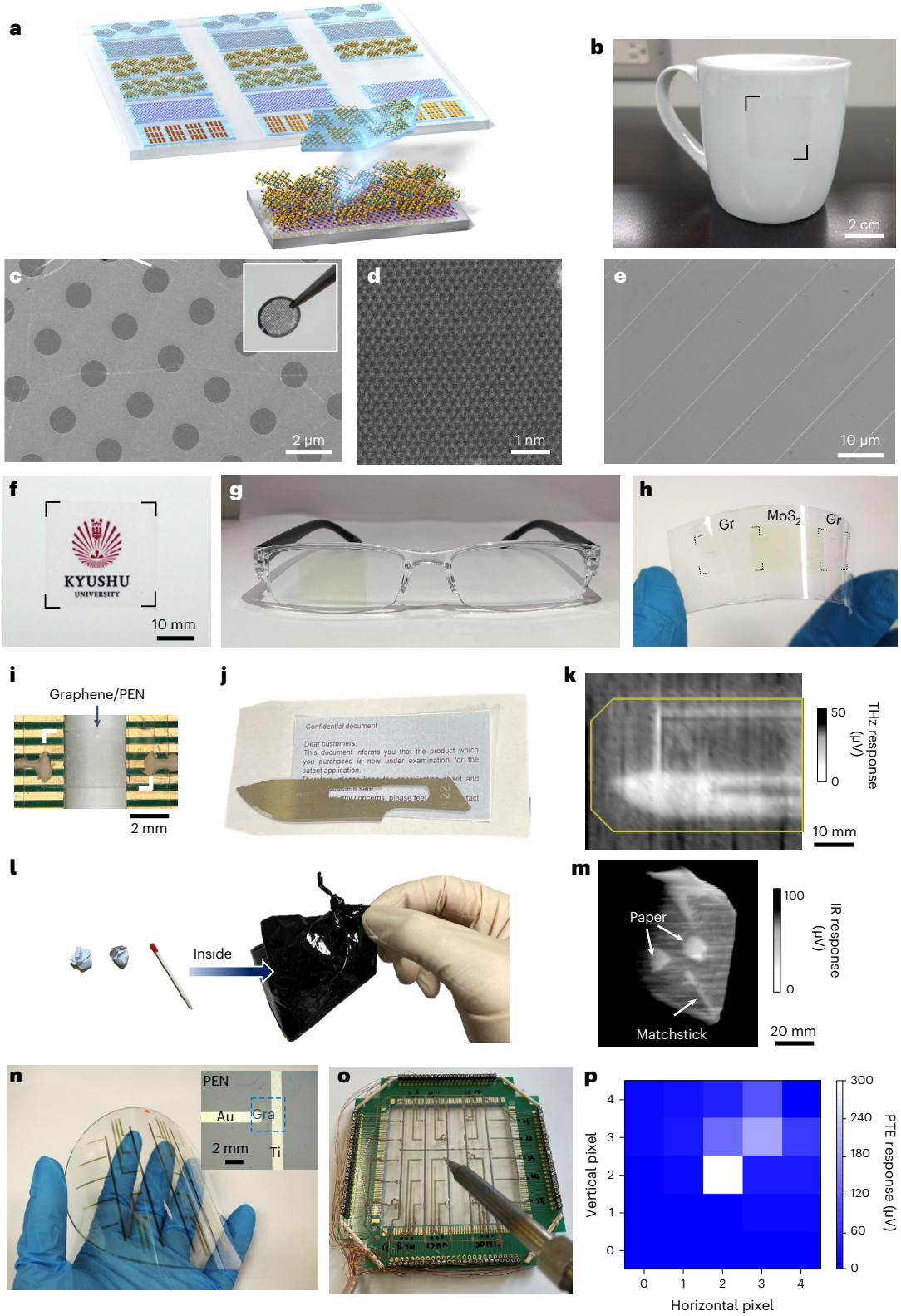

Fig. 6 | Versatility of 2D tapes and their applications. a, Illustration of a 2D tape library that can be used to transfer different 2D materials at large scale. **b**, Monolayer graphene transferred onto a ceramic mug. **c**,**d**, SEM (**c**) and STEM (**d**) images of monolayer graphene transferred onto a TEM grid. Inset in **c** is a photograph of the TEM grid with graphene. **e**, SEM image of monolayer graphene on a trenched SiO_2 substrate. **f**, Photograph of graphene transferred onto paper. **g**, Monolayer MoS_2 transferred onto curved plastic glasses. **h**, Heterostack of MoS_2 and graphene on a flexible PEN substrate. **i**, Photograph of the graphene sensor fabricated on a PEN substrate. The position of the monolayer graphene is indicated by the white guides. **j**, Materials enclosed in a paper envelope (metal blade and a piece of paper) used for THz imaging with a monolayer graphene sensor. **k**, Response image of the envelope to the THz waves ($\lambda = 577$ μm). **l**, Materials used for the IR imaging. **m**, Mapping image of the response to the IR light ($\lambda = 6.13$ μm). **n**, Photograph of a large-area thermal imaging device based on 5 × 5 graphene array fabricated on four-inch PEN substrate. **o**, Photograph showing the thermal imaging measurement. **p**, Thermal radiation-induced passive images measured by the device array. PTE, passive photo-thermoelectric.

of graphene to a delicate grid for transmission electron microscopy (TEM) (Fig. 6c,d) and to a SiO_2 substrate with micrometre-wide trenches (Fig. 6e and Supplementary Fig. 27).

It is noteworthy that after contacting the tape with a 2D material on a target substrate, the tape can be peeled off the substrate while heating at moderately low temperatures (~80 °C). In addition, the process does not require organic solvents to remove the support layer. Such a low-temperature and solvent-free release process allows us to transfer graphene and MoS_2 onto paper and plastic glasses (Fig. 6f,g and Supplementary Fig. 26b,d). In addition, it is possible to make the heterostacks of graphene and MoS_2 on a flexible polyethylene naphthalate (PEN) substrate, as shown in Fig. 6h. Overall, the UV tape has proved to have a large versatility for the transfer of 2D materials to a wide range of surfaces, even under non-ideal conditions. This flexibility makes it a reliable choice for various applications.

Monolayer graphene transferred onto a PEN substrate was used for terahertz (THz) and infrared (IR) optical sensors[32]. The voltage induced by THz waves (λ = 577 µm), passing through a paper envelope enclosing a metallic knife and a piece of paper, was monitored by the transferred graphene (Fig. 6i,j and Supplementary Fig. 28). The THz mapping clearly reveals the presence of the blade, as evidenced by a lower transmissive THz response due to the reflection of the THz waves (Fig. 6k). In addition, the edges of the paper were also detected due to the scattering of THz waves. Graphene on a PEN substrate was also employed to perform IR imaging of a matchstick and two pieces of paper stored inside a black polyethylene bag (Fig. 6l). As shown in Fig. 6m, the materials inside the bag were clearly recognized by the graphene sensor due to their higher absorbance against the IR light.

Finally, we demonstrate a thermal imaging device using a graphene pattern made on a 4 inch PEN substrate. UV tape supporting monolayer graphene was cut into 25 pieces, each 2.5 × 2.5 mm square. Each graphene piece was transferred onto the transparent PEN substrate at a predefined position to make a 5 × 5 device array connected to Ti and Au electrodes (Fig. 6n,o and Supplementary Fig. 29). The photographs shown in Fig. 6n,o display the device structure. We successfully detected far IR light emitted from a soldering iron rod with the graphene device array (Fig. 6p, Supplementary Fig. 30 and Supplementary Video 3). Even in the presence of an opaque sheet between the soldering iron rod and graphene, we could detect the IR light with the graphene sensors (Supplementary Video 4). In summary, graphene-based sensors made with the present UV tape-transfer method offer a tool for many purposes, such as security, impurity inspection, environment protection and thermal management.

Conclusions

We have reported a transfer process of 2D materials using functional tapes with adhesion force that is tuned by UV light illumination. Our method can be applied to various wafer-scale 2D materials, including monolayer graphene, BLG, TMDs and multilayer hBN, which are grown on different substrates. The surface of the transferred 2D materials is cleaner and has fewer defects and breaks compared to conventional transfer methods. The technique can also be used to make vertical stacks of multiple 2D materials and allows us to control the stacking angle, which could be further developed by automated processing. The robustness of the tape allows the 2D materials to be patterned for electronic applications while reducing the size of required materials, thus reducing material waste and lowering production cost. Furthermore, as the releasing step can be done at low temperatures without a solvent and the UV tape is mechanically flexible, 2D materials can be transferred onto various target substrates (including ceramics, paper and plastic) with different surface structures (curved surfaces and surfaces with trenches or holes). Our transfer method, which is based on ready-to-transfer 2D tape, is simple to use and could stimulate the development of electronic applications based on 2D materials.

Methods

Syntheses of 2D materials

Monolayer graphene was grown on 1-µm-thick Cu(111) film sputter deposited on c-plane sapphire (Kyocera and ADAMANT Namiki) by ambient-pressure CVD at ~1,075 °C with a mixed flow of CH_4, H_2 and Ar (refs. 21,22). Electropolished Cu foil was also used to grow a sheet of monolayer graphene. CVD BLG was grown on Cu-Ni(111) alloy film deposited on c-plane sapphire[33]. Monolayer MoS_2 (WS_2) were synthesized by reacting MoO_3 (WO_3) and sulfur on c-plane sapphire substrates in an Ar flow[34,35]. Multilayer hBN was synthesized on Fe–Ni foil (Nilaco 20 µm thickness) in a diluted flow of borazine ($B_3N_3H_6$) vapour in Ar and H_2 gases at 1,200 °C (ref. 23).

Preparation of UV tapes

Compositions of the two UV tapes and the detailed preparation methods are described in Supplementary Table 2. The adhesive force of the UV tape was measured with a peel tester (VPA-H200, Kyowa Interface Science Co.) against a Si wafer with a peeling-off speed of 300 mm min^{-1} both before and after UV illumination.

Transfer of 2D materials

For transfer of 10 × 10 mm monolayer graphene grown on a Cu(111)/sapphire substrate, we typically used a UV tape with a length of 60 mm and a width of 10 mm. After attaching the tape onto graphene using a hand roller, it was heated in an autoclave (5 atm, 50 °C) for 60 min. Then it was illuminated with UV light with an intensity of ~7 mW cm^{-2} for 75–90 sec, followed by the electrochemical delamination of the tape/graphene stack from the Cu(111) surface. After washing with deionized water, the tape/graphene was placed on a SiO_2(300 nm)/Si substrate and heated at 50–90 °C for 3 hours. Finally, the tape was peeled off the graphene while heating at 80 °C. The tape/graphene stack can be stored in a nitrogen atmosphere in the dark (Supplementary Fig. 31).

The UV tape transfer of hBN was also conducted using a method similar to that used for graphene. In the case of transfer of TMDs, UV tape/MoS_2 (or UV tape/WS_2) was peeled off the sapphire surface while soaking in water, because the intercalation of water molecules between MoS_2 and sapphire assists the delamination[10]. The details of the different UV tapes used in this study are described in Supplementary Table 2.

For PMMA-based transfer, as-grown graphene was covered with a PMMA layer by spin-coating, and the electrochemical delamination of the PMMA/graphene stack was performed. After placing the stack on a SiO_2/Si substrate, the PMMA film was removed by immersing in hot acetone (typically 80 °C, 10 hours). TRT (Nitto Denko, Revalpha No.319Y-4MS) was also used to transfer monolayer graphene. The TRT was directly attached onto the as-grown graphene on Cu(111), followed by electrochemical delamination. The TRT/graphene stack was placed on a SiO_2/Si substrate and heated at 120 °C to detach the TRT from the graphene.

Characterizations

Optical images and laser microscope images were measured with Keyence VHX-7000 and Lasertech OPTELIX, respectively. The laser microscope was effective to observe 2D materials on the tape surface. The surfaces of 2D materials were characterized by AFM and a friction force microscope (Bruker Nanoscope V and Hitachi High-Tech AFM5300). Raman and PL spectra were collected with a Tokyo Instruments Nanofinder 30 using 532 nm laser excitation. The large-area Raman mapping shown in Supplementary Fig. 23 was measured with a Renishaw inVia Qontor confocal Raman microscope using 532 nm excitation. XPS was measured with an ULVAC-PHI Quantum 2000. The cross-section of the MoS_2/WS_2 heterostacked specimen was fabricated using a focused ion beam with a Hitachi High-Tech NX-2000. Both the cross-sectional STEM images of the MoS_2/WS_2 heterostack and the top-view images of the tape-transferred monolayer graphene were measured using a JEOL Triple-C#3, an ultrahigh vacuum

ARM200F-based microscope equipped with a DELTA corrector and a cold field-emission gun operating at 60 kV. The probe current was approximately 15 pA, and the convergence semi-angle and inner acquisition semi-angle were 37 and 76 mrad, respectively. EELS core-loss spectra were obtained using a Gatan Rio CMOS camera optimized for low-voltage operation.

DFT calculations

The Vienna ab initio Simulation Package v.5.4.4 (ref. 36) was used for periodic DFT calculations for the model monomers and dimer on the graphene surface. The generalized gradient approximation described by Perdew–Burke–Ernzerhof[37] was adopted. For dispersion correction, the D3 method with the Becke–Johnson damping function[38] was employed. The Kohn–Sham equation was solved using the projector-augmented wave method[39]. The energy cutoff for the plane-wave basis set and the electronic self-consistent field threshold were set to 500 eV and 1.0×10^{-5} eV, respectively. Brillouin zone sampling on a grid with a spacing of $2\pi \times 0.05$ Å^{-1} was used. The atoms in the system were relaxed until the forces on all atoms were less than 0.05 eV Å^{-1}.

The graphene surface contains 72 carbon atoms. After adding a vacuum space of about 20 Å on the surface, geometry optimization resulted in lattice parameters of $14.80 \times 12.82 \times 20.0$ Å ($\alpha = \beta = \gamma = 90°$). The vacuum space was added to avoid interactions between periodic slabs. The obtained graphene surface was set to adsorb two monomers or one dimer. The initial structures for the DFT calculations of the adsorption structures were generated using the quench dynamics method, a means of searching for low-energy structures in conformational space. The quench dynamics simulations were performed using the Forcite module implemented in Materials Studio software, where the COMPASSIII force field[40] was used, with other computational settings described elsewhere[41]. The five most stable conformations obtained from the quench dynamics simulation were selected, and they were optimized with DFT. The structure thus obtained for each model is shown in Fig. 3b,c. Visualization of these structures was done using the VESTA software package[42].

Fabrication and measurement of 2D devices

After transferring graphene with UV tape onto a SiO_2 (300 nm)/Si substrate, photolithography and O_2 plasma treatment and electrode metal deposition were used to make channels and electrode patterns, as reported elsewhere[23]. The channel width of the graphene FETs was ~4 µm, while channel lengths of 9, 20 and 50 µm were used, with mobility showing no strong dependence on the length. Metal electrodes (Au(20 nm)/Ni(3 nm)) were deposited by electron beam evaporation, followed by lift-off. The FETs were measured at room temperature in vacuum ($<5 \times 10^{-4}$ Pa) using a Keysight Technologies B1500A semiconductor device parameter analyser.

For MoS_2 transistors (Fig. 4b), large grains of monolayer MoS_2 were used as channels. Monolayer MoS_2 samples transferred by the three different support materials—UV tape, PMMA and TRT—were used as channels for the comparison (Supplementary Fig. 21). After photolithography, Au/Ni metal electrodes were deposited, followed by lift-off. The channel length of the MoS_2 FETs was 5 µm and the channel widths were 5–20 µm as the MoS_2 grains were not patterned. The arrays of MoS_2 devices shown in Fig. 5f were fabricated by transferring cut MoS_2/tape (2.5 × 2.5 mm) onto SiO_2/Si, followed by Au electrode evaporation through a shadow mask with a channel length of 1.0 mm.

Fabrication and measurement of THz and IR sensors

Monolayer graphene was transferred onto a PEN substrate, followed by cutting into small pieces (about 3 mm × 6 mm) for attaching electrodes to use as a sensor (Fig. 6i). The fabrication process of the graphene sensor consists of wiring with conductive paste for readout electrodes, curing the electrodes at 120 °C for 10 minutes and connecting the device with a multiplexer datalogger (Keysight Technologies, 34980A-34923A/T). The readout condition of the datalogger was set to 100 nV resolution and 1 Hz scanning speed. We used a frequency multiplier (λ = 577 µm, Virginia Diodes, Custom Modular Tx-Transmitter) and a quantum cascade laser (λ = 6.13 µm, Hamamatsu Photonics, QCL L12007-1294 H-C) as the THz and IR sources, respectively. The graphene channel-ground electrode interface serves as the photo-detection interface. The device exhibits direct current voltage signals against external irradiation under photo-thermoelectric effect. The THz and IR imaging measurements are transmissive mode, and this work utilized motorized digital stepping stages and a stage controller to manage the spatial positions of the imaging targets. The stepping unit was set to 1 mm. Detailed experimental conditions can be found elsewhere[43,44].

Fabrication and measurement of passive photo-thermal imaging devices

The UV tape supporting monolayer graphene was cut into small pieces (2.5 × 2.5 mm). The 25 pieces were attached to a 4 inch PEN substrate at fixed positions to make a 5 × 5 array, followed by removing all the tapes. Then, Ti and Au electrodes were separately deposited by electron beam deposition using two different metal masks (Fig. 6n and Supplementary Fig. 29). In the passive imaging measurements, we used a commercial soldering iron rod (Quick Heat soldering iron, TQ-95, Taiyo Electric Ind. Co. Ltd.) as a thermal radiation source. The device array was controlled with LabVIEW software, and the passive photo-thermoelectric images were processed using Origin software.

Data availability

The data that support the findings of this study are available from the corresponding author upon reasonable request.

References

1. Ferrari, A. C. et al. Science and technology roadmap for graphene, related two-dimensional crystals, and hybrid systems. *Nanoscale* **7**, 4598–4810 (2015).
2. Ago, H. et al. Science of 2.5 dimensional materials: paradigm shift of materials science toward future social innovation. *Sci. Tech. Adv. Mater.* **23**, 275–299 (2022).
3. Ullah, S. et al. Graphene transfer methods: a review. *Nano Res.* **14**, 3756–3772 (2021).
4. Gao, Y. et al. Recent progress in the transfer of graphene films and nanostructures. *Small Methods* **5**, 2100771 (2021).
5. Kim, J. Y. van der Waals layer transfer of 2D materials for monolithic 3D electronic system integration: review and outlook. *ACS Nano* **17**, 1831–1844 (2023).
6. Chen, T.-A. et al. Wafer-scale single-crystal hexagonal boron nitride monolayers on Cu (111). *Nature* **579**, 219–223 (2020).
7. Li, T. et al. Epitaxial growth of wafer-scale molybdenum disulfide semiconductor single crystals on sapphire. *Nat. Nanotechnol.* **16**, 1201–1207 (2021).
8. Li, X. et al. Transfer of large-area graphene films for high-performance transparent conductive electrodes. *Nano Lett.* **9**, 4359–4363 (2009).
9. Lian, X. et al. Toward clean and crackless transfer of graphene. *ACS Nano* **5**, 9144–9153 (2011).
10. Gurarslan, A. et al. Surface-energy-assisted perfect transfer of centimeter-scale monolayer and few-layer MoS_2 films onto arbitrary substrates. *ACS Nano* **8**, 11522–11528 (2014).
11. Leong, W. S. et al. Paraffin-enabled graphene transfer. *Nat. Commun.* **10**, 867 (2019).
12. Zhang, Z. et al. Rosin-enabled ultraclean and damage-free transfer of graphene for large-area flexible organic light-emitting diodes. *Nat. Commun.* **8**, 14560 (2017).
13. Hung, Y.-H. Ultraclean and facile patterning of CVD graphene by a UV-light-assisted dry transfer method. *ACS Appl. Mater. Interfaces* **15**, 4826–4834 (2023).

14. Zhao, Y. et al. Large-area transfer of two-dimensional materials free of cracks, contamination and wrinkles via controllable conformal contact. *Nat. Commun.* **13**, 4409 (2022).
15. Kang, J. et al. Efficient transfer of large-area graphene films onto rigid substrates by hot pressing. *ACS Nano* **6**, 5360–5365 (2012).
16. Ryu, J. et al. Fast synthesis of high-performance graphene films by hydrogen-free rapid thermal chemical vapor deposition. *ACS Nano* **8**, 950–956 (2014).
17. Kim, H. et al. High-throughput manufacturing of epitaxial membranes from a single wafer by 2D materials-based layer transfer process. *Nat. Nanotechnol.* **18**, 464–470 (2023).
18. Pizzocchero, F. et al. The hot pick-up technique for batch assembly of van der Waals heterostructures. *Nat. Commun.* **7**, 11894 (2017).
19. Masubuchi, S. et al. Autonomous robotic searching and assembly of two-dimensional crystals to build van der Waals superlattices. *Nat. Commun.* **9**, 1413 (2018).
20. Mannix, A. J. Robotic four-dimensional pixel assembly of van der Waals solids. *Nat. Nanotechnol.* **17**, 361–366 (2022).
21. Hu, B. et al. Epitaxial growth of large-area single-layer graphene over Cu(111)/sapphire by atmospheric pressure CVD. *Carbon* **50**, 57–65 (2012).
22. Ago, H. et al. Epitaxial growth and electronic properties of large hexagonal graphene domains on Cu(111) thin film. *Appl. Phys. Express* **6**, 075101 (2013).
23. Fukamachi, S. et al. Large-area synthesis and transfer of multilayer hexagonal boron nitride for enhanced graphene device arrays. *Nat. Electron.* **6**, 126–136 (2023).
24. Higuchi, C. et al. Molecular understanding of the adhesive interactions between silica surface and epoxy resin: effects of interfacial water. *J. Comput. Chem.* **40**, 164–171 (2019).
25. Tsuji, Y. et al. Theoretical study on the adhesion interaction between epoxy resin including curing agent and plated gold surface. *Langmuir* **37**, 3982–3995 (2021).
26. Hong, X. et al. Ultrafast charge transfer in atomically thin MoS_2/WS_2 heterostructures. *Nat. Nanotechnol.* **9**, 682–686 (2014).
27. Banszerus, L. et al. Ultrahigh-mobility graphene devices from chemical vapor deposition on reusable copper. *Sci. Adv.* **1**, e1500222 (2015).
28. Lee, J. E. et al. Optical separation of mechanical strain from charge doping in graphene. *Nat. Commun.* **3**, 1024 (2012).
29. Kireev, D. et al. High throughput transfer technique: save your graphene. *Carbon* **107**, 319–324 (2016).
30. Kim, K. et al. van der Waals heterostructures with high accuracy rotational alignment. *Nano Lett.* **16**, 1989–1995 (2016).
31. Solís-Fernández, P. & Ago, H. Machine learning determination of the twist angle of bilayer graphene by Raman spectroscopy: implications for van der Waals heterostructures. *ACS Appl. Nano Mater.* **5**, 1356–1366 (2022).
32. Araki, T. et al. Broadband photodetectors and imagers in stretchable electronics packaging. *Adv. Mater*. 202304048 (2023).
33. Takesaki, Y. et al. Highly uniform bilayer graphene on epitaxial Cu–Ni(111) alloy. *Chem. Mater.* **28**, 4583–4592 (2016).
34. Suenaga, K. et al. Surface-mediated aligned growth of monolayer MoS_2 and in-plane heterostructures with graphene on sapphire. *ACS Nano* **12**, 10032–10044 (2018).
35. Ji, H. G. et al. Hydrogen-assisted epitaxial growth of monolayer tungsten disulfide and seamless grain stitching. *Chem. Mater.* **30**, 403–411 (2018).
36. Kresse, G. et al. Efficient iterative schemes for *ab initio* total-energy calculations using a plane-wave basis set. *Phys. Rev. B* **54**, 11169–11186 (1996).
37. Perdew, J. P. et al. Generalized gradient approximation made simple. *Phys. Rev. Lett.* **77**, 3865–3868 (1996).
38. Grimme, S. et al. Effect of the damping function in dispersion corrected density functional theory. *J. Comput. Chem.* **32**, 1456–1465 (2011).
39. Kresse, G. et al. From ultrasoft pseudopotentials to the projector augmented-wave method. *Phys. Rev. B* **59**, 1758–1775 (1999).
40. Sun, H. et al. COMPASS II: extended coverage for polymer and drug-like molecule databases. *J. Mol. Model.* **22**, 47 (2016).
41. Tsuji, Y. et al. Competition between hydrogen bonding and dispersion force in water adsorption and epoxy adhesion to boron nitride: from the flat to the curved. *Langmuir* **37**, 11351–11364 (2021).
42. Momma, K. et al. VESTA 3 for three-dimensional visualization of crystal, volumetric and morphology data. *J. Appl. Crystallogr.* **44**, 1272–1276 (2011).
43. Li, K. et al. Robot-assisted, source-camera-coupled multi-view broadband imagers for ubiquitous sensing platform. *Nat. Commun.* **12**, 3009 (2021).
44. Li, K. et al. Stretchable broadband photo-sensor sheets for nonsampling, source-free, and label-free chemical monitoring by simple deformable wrapping. *Sci. Adv.* **8**, eabm4349 (2022).

Acknowledgements

This work was supported by New Energy and Industrial Technology Development Organization (NEDO) grant no. JPNP14004, JSPS Grant-in-Aid for Scientific Research on Innovative Areas 'Science of 2.5 Dimensional Materials: Paradigm Shift of Materials Science Toward Future Social Innovation' (KAKENHI grant nos. JP21H05232, JP21H05233, JP21H05235, 22H05470 and 22H05478) and JST CREST grant nos. JPMJCR18I1 and JPMJCR20B1. H.A. acknowledges KAKENHI grant nos. 23K18878, JP19K22113 and JP18H03864; Y.T. acknowledges KAKENHI grant nos. JP21K04996 and JP22H05146; and Q.L. acknowledges KAKENHI grant no. JP22F22358. Y.K. acknowledges JST Mirai program grant no. JPMJMI23G1 and Strategic Research Development Program of the Kanagawa Institute of Industrial Science and Technology. The computations in this work were performed using the computer facilities at the Research Institute for Information Technology, Kyushu University and at the Supercomputer Center, the Institute for Solid State Physics, the University of Tokyo. We acknowledge H. Nakano for help with the graphene transfer, Z. Ma for the MoS_2 growth, T. Matsunaga for the BLG and MoS_2 synthesis and transfer, H. Sun for the STEM analaysis, H. Tomori for the fabrication of trench arrays and D. Shikichi, Y. Matsuzaki, S. Hirokawa and R. Ota for help with the THz and IR measurements.

Author contributions

H.A., A.Y., M.N., S.F., P.S.-F., K.K. and S.H. designed the experiments. K.K. and M.N. prepared the graphene, S.F. prepared the hBN and M.K. and A.U. prepared the MoS_2 and WS_2. M.N., S.H., S.F., K.K., M.K., S.O., H.G.J., A.U. and P.S.-F. performed the tape transfer and analysed the transferred 2D materials. M.N., S.F. and P.S.-F. fabricated and measured the FETs. Y.T., Y.S. and K.Y. performed the DFT calculations. Q.L., Y.-C.L. and K.S. performed STEM measurement. K.L. and Y.K. fabricated and measured the THz and IR sensors. H.A., P.S.-F., Y.T., Y.S., Y.-C.L. and K.L. wrote the paper. All the authors discussed the data and results.

Competing interests

The authors declare no competing interests.

Additional information

Extended data is available for this paper at https://doi.org/10.1038/s41928-024-01121-3.

Supplementary information The online version contains supplementary material available at https://doi.org/10.1038/s41928-024-01121-3.

Correspondence and requests for materials should be addressed to Hiroki Ago.

Peer review information *Nature Electronics* thanks Weida Hu, Ching-Yuan Su and the other, anonymous, reviewer(s) for their contribution to the peer review of this work.

https://doi.org/10.1038/s41928-024-01121-3

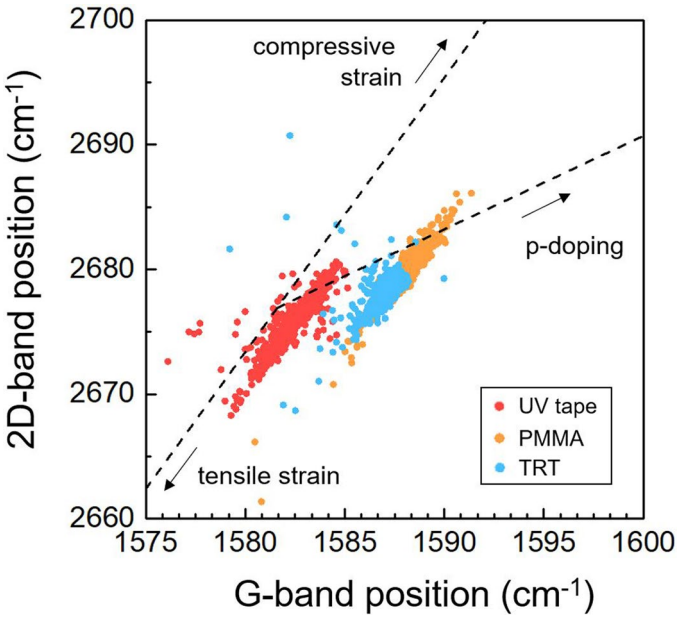

Extended Data Fig. 1 | Comparison of doping and strain induced by the graphene transfer processes. Raman 2D and G band positions are plotted to clarify the doping and strain in the transferred graphene. The p-type doping induced by PMMA and TRT is strongly suppressed in the UV tape-transferred graphene, while there is no essential difference in strain.

https://doi.org/10.1038/s41928-024-01121-3

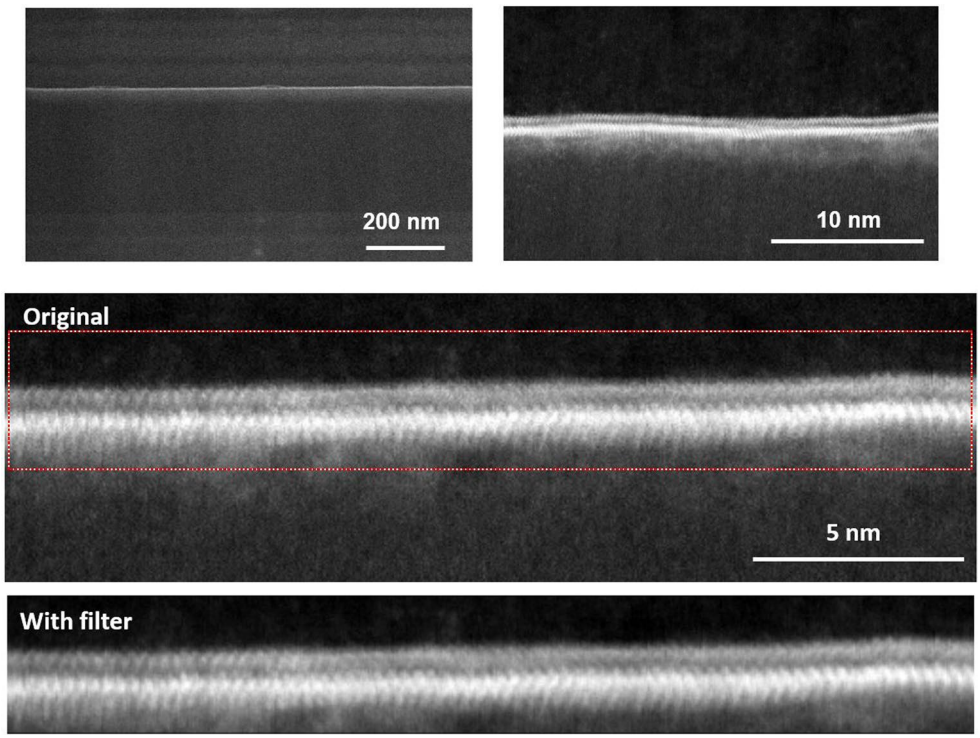

Extended Data Fig. 2 | STEM images of the MoS_2/WS_2 heterostack. Cross-sectional STEM images of the MoS_2/WS_2 heterostack with different magnifications. The images show a clean interface between the MoS_2 and WS_2 monolayers, supporting the effectiveness of the tape transfer for making vertical heterostacks of various 2D materials.

https://doi.org/10.1038/s41928-024-01121-3

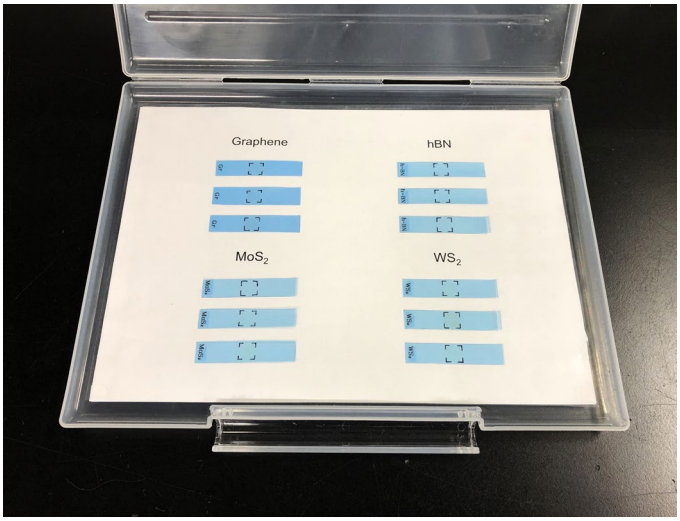

Extended Data Fig. 3 | Library of 2D materials tapes. Photograph of tapes already having monolayer graphene, multilayer hBN, monolayer MoS_2 and monolayer WS_2 on them. As the tape used for graphene and others are different, the color of the graphene tape looks slightly different. These tapes are ready to transfer the 2D materials onto various substrates after heating at 50–90 °C, followed by removing the tape.